

# A MECHANISTIC CRITICAL HEAT FLUX MODEL FOR SUBCOOLED FLOW BOILING BASED ON LOCAL BULK FLOW CONDITIONS

C. H. LEE† and I. MUDAWWAR

Boiling and Two-phase Flow Laboratory, School of Mechanical Engineering, Purdue University,  
West Lafayette, IN 47907, U.S.A.

(Received 25 December 1987; in revised form 10 July 1988)

**Abstract**—The critical heat flux (CHF) mechanisms for subcooled flow boiling are reviewed. Based on experimental observations reported by previous investigators, the authors have developed a new mechanistic CHF model for vertical subcooled flow at high pressure and high mass velocity. This model is based on the dryout of a thin liquid layer (sublayer) beneath an intermittent vapor blanket due to a Helmholtz instability at the sublayer–vapor interface. The parametric trends of CHF have been explored qualitatively and quantitatively with respect to variations in pressure, mass velocity, subcooling and tube diameter. Comparisons of the model predictions with experimental data for water show good agreement in the simulation of subcooled flow conditions of pressurized water reactors (PWRs).

**Key Words:** CHF, boiling, dryout, sublayer, prediction

## 1. INTRODUCTION

Subcooled flow boiling systems are commonly encountered in high heat flux applications such as nuclear reactor cores, accelerator targets and advanced microelectronic cooling modules. The operating conditions in these applications are designed to maintain heat fluxes lower than the critical heat flux (CHF) for preventing potential failure by overheating or burnout. For subcooled flow, CHF is a condition in which a small increase in heat flux leads to abrupt wall overheating caused by the transition from nucleate to film boiling.

The CHF phenomenon has been researched extensively during the last three decades, especially in relation to the thermal-hydraulics of nuclear reactors. Although numerous empirical and semi-empirical CHF correlations have been presented for subcooled flow boiling at high pressure and high mass velocity, strong disagreements still exist among various investigators about the following issues:

1. The physical picture of subcooled flow boiling just before CHF.
2. The conditions that trigger CHF.
3. The controlling factors determining CHF variations with respect to pressure, mass velocity, subcooling and hydraulic diameter.

This paper summarizes the CHF mechanisms for subcooled flow boiling. The observations of many investigators are used to help develop a new mechanistic CHF model for high pressure and high mass velocity. The accuracy of the present model is evaluated by comparing model predictions with experimental data for water. Finally, the controlling factors for determining the CHF trends are discussed in detail.

## 2. BACKGROUND

Several comprehensive reviews of worldwide research on CHF have been published (Tong 1972; Tong & Hewitt 1972; Bergles 1977, 1979; Hewitt 1978; Theofanous 1980; Kitto 1980; Groeneveld & Snoek 1984). The following review, however, focuses more on the mechanisms and theoretical predictions of CHF in subcooled flow boiling.

---

†Present address: Institute of Nuclear Energy Research, P. O. Box 3-3, Lung-Tan, Taiwan 32500, R.O.C.

### 2.1. Review of CHF Mechanisms

In general, CHF in subcooled flow boiling is associated with the departure from nucleate boiling (DNB) to film boiling. CHF mechanisms are usually studied by optical techniques to understand the liquid-vapor flow configuration near the wall and in the bulk region, and by wall temperature measurements which record the unsteady temperature excursions associated with CHF.

Fiori & Bergles (1970) observed that, just prior to CHF, the wall temperature increased periodically when bubbles moving past nucleation sites interrupted the supply of liquid to the wall. CHF occurred where the wall temperature exceeded the Leidenfrost temperature and prevented rewetting. They postulated that the thickness of the wall liquid sublayer was quite large, and the water mass entering the sublayer was still greater than the mass evaporating at the wall.

Molen & Galjee (1978), however, emphasized the effect of liquid sublayer evaporation on CHF. They maintained that, at CHF, a very thin liquid layer beneath a coalescent bubble or vapor slug can be evaporated in a few milliseconds while the passage time of a vapor slug is about 0.1 s.

Hino & Ueda (1985) observed that remarkably large coalescent bubbles appeared periodically at high heat fluxes, and that CHF occurred because of liquid sublayer dryout beneath the coalescent bubbles. They indicated that the large temperature rise associated with CHF resulted from periodic and unsteady overheating of the wall beyond the Leidenfrost temperature.

Mattson *et al.* (1973) presented photographic results of subcooled flow boiling CHF at high pressure, high mass velocity and medium or low subcooling. They observed that the bubbles growing on the heated wall moved along the wall before departing into the subcooled liquid. Bubbles were relatively small at high pressure and high mass velocity. The largest bubble was generated by the coalescence of smaller bubbles within the bubble boundary layer. They indicated that there was no abrupt visible change in the macroscopic two-phase bulk flow pattern at CHF. Yet, the heated surface seemed to develop a thin continuous vapor layer due to bubble coalescence within the bubble boundary layer.

### 2.2. Review of Semi-empirical Models

Several semi-empirical CHF models have been reported during the last three decades. Typically, bubble layer separation, near-wall bubble "crowding" and sublayer dryout have been proposed as CHF mechanisms in the development of these models.

#### 2.2.1. Boundary layer separation models

The boundary layer separation models are based on the assumption that vapor "injection" into the liquid stream reduces the liquid velocity gradient near the wall. The liquid separates from the wall, resulting in a transition from nucleate to film boiling when the rate of vapor effusion increases beyond a critical level. Semi-empirical CHF correlations, based on the bubble boundary layer separation concept, have been developed by Kutateladze (1966), Tong (1968, 1975), Purcupile & Gouse (1972), Smogalev (1981) and others.

The boundary layer separation mechanism has lost its popularity in recent years. The high-pressure experiments of Mattson *et al.* (1973) and the low-pressure studies of Fiori & Bergles (1970), Molen & Galjee (1978) and Hino & Ueda (1985) demonstrate the weak physical basis on which it was developed.

#### 2.2.2. Near-wall bubble crowding models

Weisman & Pei (1983) presented a CHF model for high mass velocity in tubes. Turbulent interchange between the bubbly layer and core regions was considered the limiting mechanism for the onset of CHF. The void fraction in the bubbly layer was determined by a balance between the outward vapor flow away from the wall and the inward liquid flow at the bubbly layer-core interface. They postulated that CHF occurs when the void fraction in the bubbly layer just exceeds the critical value of 0.82. The void fraction was calculated under the assumption of homogeneous two-phase flow in the bubbly layer.

Weisman & Ying (1983) extended the work of Weisman & Pei to low mass velocities, using the slip model instead of the homogeneous flow model. In 1985, they presented theoretical CHF predictions for rod bundles with uniform or nonuniform axial heat fluxes at PWR conditions.

Contrary to Weisman & Pei's assumption, Styrikovich *et al.* (1970) have shown that the local critical void fraction at the wall near CHF varied from 0.3 to 0.95, depending on the degree of subcooling, mass velocity and pressure. Lahey & Moody (1977) proposed using a void profile-fit method such as Levy's (1966) to predict the void fraction near the wall. That technique, however, was based on uniform axial heat flux data and, as such, its predictions cannot be confirmed for nonuniform axial heat flux applications.

### 2.2.3. Sublayer dryout models

Haramura & Katto (1983) presented a CHF model for both pool and forced convection boiling on submerged bodies in a saturated liquid. CHF was assumed to occur when: (1) a vapor blanket isolates the heated surface from bulk liquid cooling leaving a thin liquid layer (sublayer) at the wall; and (2) the liquid entering the sublayer falls short of balancing the rate of sublayer dryout by evaporation. The thickness of the sublayer was determined by the critical wavelength associated with the Helmholtz instability of vapor jets leaving the wall. Their model, however, did not include the effect of subcooling on CHF.

Serizawa (1983) presented a model for CHF during a power increase. The maximum heat flux was based on a balance between the consumption of the sublayer, which is formed between a vapor blanket and the heated surface, and the supply of liquid during a postulated transient. The steady-state sublayer thickness, related to single bubble growth and bubble distribution, was presented as an empirical correlation for low-pressure conditions.

The sublayer dryout models are strongly by more recent experimental studies on flow boiling CHF. The observations by Mesler (1976), Molen & Galjee (1978), Bhat *et al.* (1983), Serizawa (1983), Hino & Ueda (1985) and Mudawwar *et al.* (1987) represent strong evidence that, just before CHF, a very thin liquid sublayer is trapped beneath a blanket formed by the coalescence of several bubbles at the heated wall. CHF reported occurred due to dryout of the sublayer, causing an unsteady rise of wall temperature. The study by Mattson *et al.* (1973) further suggests that the two-phase bulk flow does not undergo an abrupt visible change in flow pattern at the onset of CHF at high pressure and high mass velocity. Thus, to predict the combination of bulk flow conditions which triggers CHF, it is sufficient to model the influence of these conditions on the formation and dryout of the liquid sublayer within the bubble boundary layer at the wall. This rationale is the basis for the new mechanistic CHF model presented in this paper.

## 3. CHF MODEL

Figure 1 represents the boiling configuration of subcooled flow immediately before and just after CHF, based on the experimental observations reported by earlier investigators. The present authors propose a new CHF model based on the following assumptions:

1. Vapor blankets are formed from small bubbles piling up as vertical distorted vapor cylinders. The development of each blanket is strongly influenced by neighboring blankets which tend to confine its circumferential growth and to prevent liquid from entering the sublayer from the sides of the blanket. Thus, it is assumed that the equivalent diameter of each blanket is approximately equal to the diameter of a bubble upon departure from the wall. The departing bubbles are assumed to coalesce into a distorted blanket, which maintains a fairly constant equivalent diameter while stretching in the direction of fluid flow due to the generation of more vapor by sublayer evaporation. Neighboring blankets may ultimately merge circumferentially to form a continuous blanket on the inner wall of the tube.
2. The velocity of the vapor blanket in the turbulent flow stream is assumed to be the superposition of the local liquid velocity and the relative vapor blanket velocity, determined by a balance between the buoyancy and drag forces exerted on the blanket.
3. The thin liquid sublayer beneath the blanket is interrupted by the formation of a dry patch after a Helmholtz instability at the sublayer-blanket interface (see

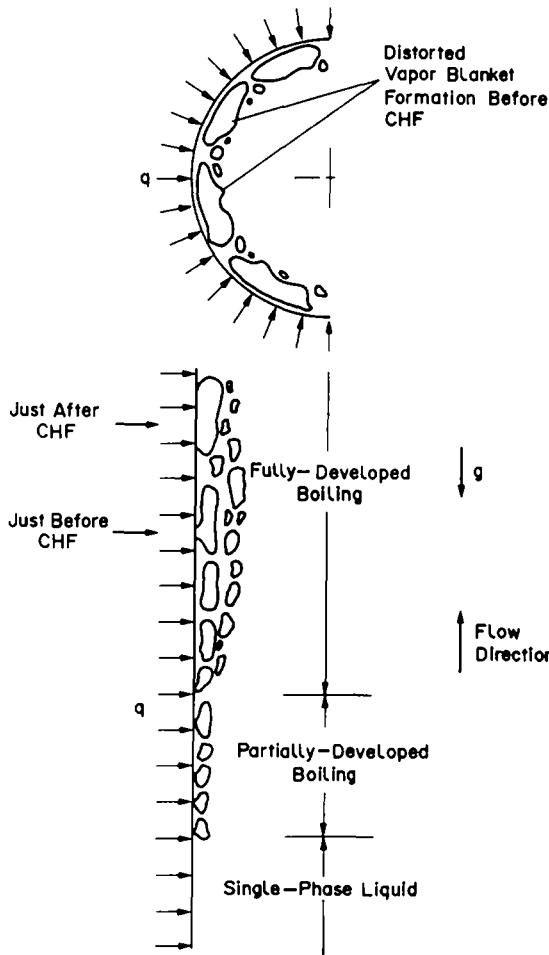


Figure 1. Subcooled flow CHF at high pressure and high mass velocity.

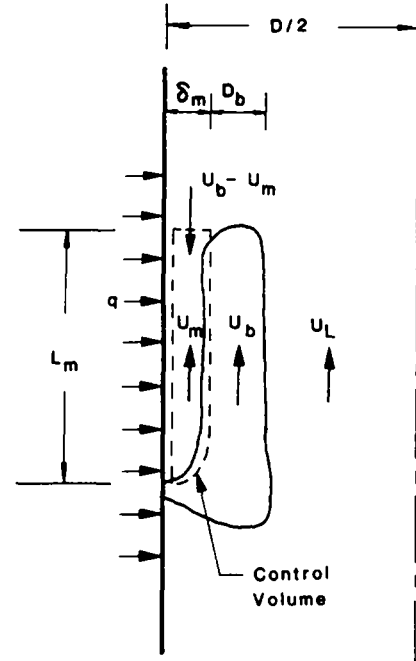


Figure 2. Schematic representation of the onset of sublayer dryout.

figure 2). The length of the blanket is assumed to be equal to the critical Helmholtz wavelength.

4. CHF occurs when the rate of sublayer mass loss by evaporation exceeds that of the liquid entering the sublayer from the core region.

Figure 2 shows a schematic diagram of a control volume which surrounds the sublayer and moves at the same velocity as the vapor blanket. Near CHF the vapor blanket touches the heated wall as a result of the Helmholtz instability. The dry patch persists and spreads very quickly over the wall if the enthalpy of the subcooled liquid entering the sublayer falls short of balancing fluid evaporation at the wall. That is,

$$q_{\text{CHF}} D_b L_m = D_b G_m \delta_m [h_{\text{LG}} + c_{\text{PL}}(T_{\text{sat}} - T_m)], \quad [1]$$

where  $q_{\text{CHF}}$  is the critical heat flux,  $D_b$  is the equivalent diameter of the vapor blanket,  $L_m$  is the length of the sublayer (or vapor blanket),  $\delta_m$  is the sublayer thickness,  $G_m$  is the relative mass velocity of liquid entering the sublayer,  $h_{\text{LG}}$  is the latent heat of vaporization,  $c_{\text{PL}}$  is the specific heat of the liquid,  $T_{\text{sat}}$  is the saturated temperature of liquid and  $T_m$  is the temperature of the liquid entering the sublayer. The subcooling of the liquid entering the sublayer can be approximated as

$$T_{\text{sat}} - T_m = a_1 (T_{\text{sat}} - T_L), \quad [2]$$

where  $a_1$  is an empirical constant and  $T_L$  is the local mean bulk temperature of the subcooled liquid. After [1] and [2] are combined, the critical heat flux reduces to

$$q_{CHF} = \frac{G_m \delta_m [h_{LG} + a_1 c_{PL} (T_{sat} - T_L)]}{L_m} \quad [3]$$

Thus to determine CHF, parametric relations are needed for the sublayer thickness, the relative sublayer mass velocity and the length of the sublayer. The functional dependences of these variables are presented in the following sections.

It should be emphasized that the proposed model is mechanistic in nature and that it describes a specific process associated with CHF. Nevertheless, the development of the model will require the use of available correlations to describe the dynamics of bubbles in the wall region. Although the accuracy of the model depends on the reliability of these individual correlations, the model can be easily adjusted to accommodate the use of other correlations the reader may find more suitable for a specific range of operating conditions. The semi-empirical formulation of CHF in the present study was accomplished by testing several empirical correlations to assess the effect of these correlations on the overall accuracy of the model.

### 3.1. Sublayer Mass Velocity and Vapor Blanket Length

Near the CHF condition, the vapor blanket is formed by the coalescence of the small bubbles. The blanket is assumed to be a distorted cylinder with length  $L_m$  and equivalent diameter  $D_b$  which forms a flat interface near the wall. The velocity of the vapor blanket in vertical turbulent flow is determined by a balance between the buoyancy force  $F_B$  and the drag force  $F_D$ :

$$F_B + F_D = 0, \quad [4]$$

where

$$F_B = \frac{\pi}{4} D_b^2 L_m \Delta \rho g \quad [5]$$

and

$$F_D = -\frac{1}{2} \rho_L C_D (U_b - U_{bL})^2 \frac{\pi D_b^2}{4} \quad [6]$$

where  $\Delta \rho$  is equal to  $\rho_L - \rho_G$ , the density difference between the two phases, and  $C_D$  is the drag coefficient. The negative sign in [6] indicates that the direction of the drag force is opposite the flow direction.

Two different equations for the bubble drag coefficient were tested in the present study. The first was recommended by Harmathy (1960) and Ishii & Zuber (1979) for a deformed bubble whose motion is determined by buoyancy and surface tension forces. Chan & Prince (1965) proposed a different equation for small bubbles. They indicated that the motion of a very small deformed bubble is dominated by viscous forces; yet, they did not specifically propose using their equation for slender cylindrical bubbles. The use of the Chan & Prince equation in the present analysis is justified by the small bubble size associated with high-pressure systems typical of PWR conditions.

Drag coefficients based on these two references are as follows:

$$\text{Harmathy,} \quad C_D = \frac{2}{3} \frac{D_{eb}}{\left(\frac{\sigma}{g \Delta \rho}\right)^{0.5}}; \quad [7a]$$

and

$$\text{Chan \& Prince,} \quad C_D = \frac{48 \mu_L}{\rho_L D_{eb} (U_b - U_{bL})}; \quad [7b]$$

where  $\mu_L$  is the liquid viscosity,  $\sigma$  is the surface tension,  $(U_b - U_{bL})$  is the relative velocity of the bubble with respect to the liquid at a position corresponding to the centerline of the bubble and  $D_{eb}$  is the equivalent diameter of the bubble.

Since the vapor blanket is formed initially by the coalescence of a vertical column of small bubbles and is confined against circumferential growth by the neighboring blankets, it is postulated

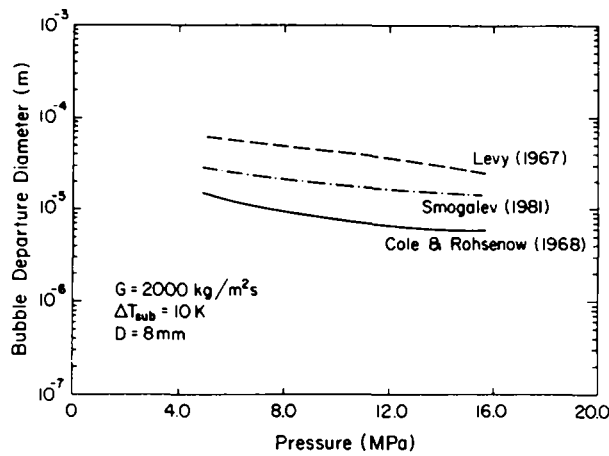


Figure 3. Bubble departure diameter predictions based on the models of Levy (1967), Cole & Rohsenow (1968) and Smogalev (1981).

that the equivalent blanket diameter,  $D_{eb}$ , is approximately equal to the departure diameter,  $D_b$ , of the coalescing bubbles. The present model was formulated using the departure diameter models of Levy (1967), Cole & Rohsenow (1968) and Smogalev (1981).

The Levy model is based on a balance between surface tension and shear forces created by liquid motion on a bubble in contact with the wall. Cole & Rohsenow proposed an alternative correlation for predicting  $D_b$  in pool boiling based on water data obtained over a very wide range of pressure. Their correlation is also applicable to forced convection systems where the shear force is much smaller than the buoyancy force. Smogalev extended the low-pressure bubble departure diameter equation of Koumoutsos *et al.* (1968) to forced convection boiling of water at high pressure. Figure 3 shows the Cole & Rohsenow model predicting much smaller bubble diameters compared to other two models.

Bubble diameters based on the three references are as follows:

Levy,

$$D_b = 0.015 \left( \frac{\sigma D}{\tau_w} \right)^{0.5}; \quad [8a]$$

Cole & Rohsenow,

$$D_b = 1.5 \times 10^{-4} \left( \frac{\sigma}{g \Delta \rho} \right)^{0.5} \left( \frac{\rho_L c_{PL} T_{sat}}{\rho_G h_{LG}} \right)^{1.25}; \quad [8b]$$

and

Smogalev,

$$D_b = 0.0208 \left( \frac{\sigma}{g \Delta \rho} \right)^{0.5} \left[ 1 - 0.65 (P_{cr} - P)^3 \frac{\rho_G v_L G}{\rho_L \sigma g} \right]^2; \quad [8c]$$

where  $\tau_w (= fG^2/2\rho_L)$  is the wall shear stress based on the Fanning friction factor,  $f (= 0.046 \text{Re}^{-0.2})$ , for pure liquid flowing at Reynolds number  $\text{Re}$  in a tube of diameter  $D$ , and  $G$ ,  $v_L$ ,  $P$  and  $P_{cr}$  are, respectively, the liquid mass velocity, the liquid kinematic viscosity, the local static pressure (MPa) and the critical pressure.

Combining [4]–[7] gives the velocity of the vapor blanket:

$$U_b = \left( \frac{2L_m g \Delta \rho}{\rho_L C_D} \right)^{0.5} + U_{bl}. \quad [9]$$

The velocity profile for turbulent flow through a tube can be represented by the three-layer distribution of mainstream liquid velocity  $U_L$  as a function of distance  $y$  from the wall (Arpaci &

Larsen 1984),

$$U_L^+ = y^+, \quad 0 \leq y^+ < 5, \quad [10a]$$

$$U_L^+ = 5 \ln y^+ - 3.05, \quad 5 \leq y^+ < 30, \quad [10b]$$

$$U_L^+ = 2.5 \ln y^+ + 5.5, \quad y^+ \geq 30, \quad [10c]$$

where

$$U_L^+ \equiv \frac{U_L}{U_\tau}, \quad [10d]$$

$$y^+ \equiv y \frac{U_\tau}{\nu_L} \quad [10e]$$

and

$$U_\tau \equiv \left( \frac{\tau_w}{\rho_L} \right)^{0.5}, \quad [10f]$$

where  $U_L^+$  is the dimensionless liquid velocity,  $y^+$  is the dimensionless distance from the wall and  $U_\tau$  is the friction velocity.

The authors found the liquid velocity profile around the vapor blanket to belong to the buffer region, [10b], for all the simulated PWR conditions of the present study. The mean velocity of the liquid at distance  $y = \delta_m + D_b/2$  from the wall is given by

$$U_{bL} = 0.758 \text{ Re}^{0.1} \frac{G}{\rho_L} \left\{ \ln \left[ \frac{0.152 \text{ Re}^{-0.1} G \left( \delta_m + \frac{D_b}{2} \right)}{\mu_L} \right] - 0.61 \right\}. \quad [11]$$

Combining [9] and [11] gives the vapor blanket velocity as

$$U_b = \left( \frac{2L_m g \Delta \rho}{\rho_L C_D} \right)^{0.5} + 0.758 \text{ Re}^{-0.1} \frac{G}{\rho_L} \left\{ \ln \left[ \frac{0.152 \text{ Re}^{-0.1} G \left( \delta_m + \frac{D_b}{2} \right)}{\mu_L} \right] - 0.61 \right\}. \quad [12]$$

Since CHF is postulated to occur as a result of the Helmholtz instability, the lengths of the sublayer and vapor blanket are assumed to be equal to the critical Helmholtz wavelength, as shown in figure 2, i.e.

$$L_m = \frac{2\pi\sigma(\rho_L + \rho_G)}{\rho_L \rho_G (U_b - U_m)^2}. \quad [13]$$

The relative microlayer mass velocity and the length of the vapor blanket can be further simplified since the liquid velocity in the sublayer is small in comparison to the velocity of the vapor blanket, i.e.

$$G_m = \rho_L U_b \quad [14]$$

and

$$L_m \cong \frac{2\pi\sigma(\rho_L + \rho_G)}{\rho_L \rho_G U_b^2}, \quad [15]$$

where  $U_b$  is obtained from [12].

### 3.2. Sublayer Thickness

Figure 4 shows that the thickness of the liquid sublayer is determined by a force balance on the vapor blanket in the radial direction. Vapor generation from sublayer evaporation creates a rate of momentum,  $\dot{M}_1$ , into the vapor blanket, which pushes the vapor blanket away from the wall.

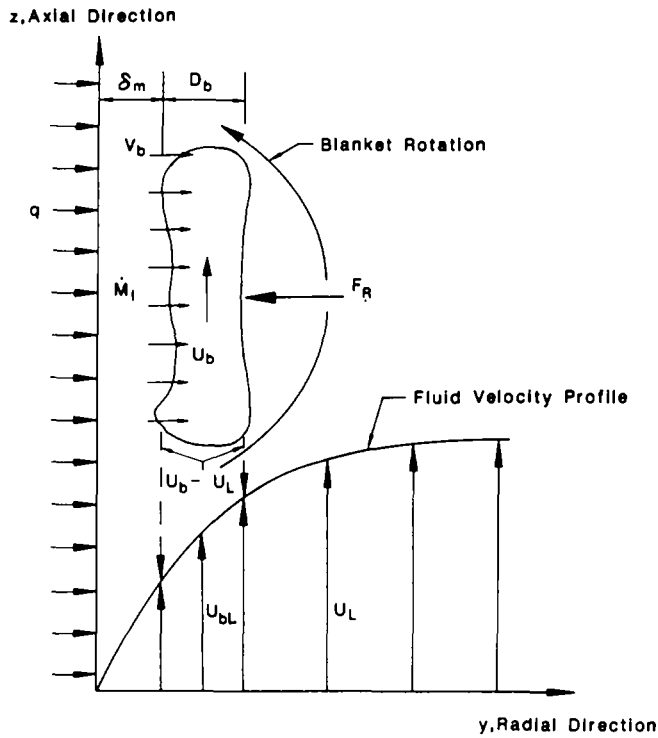


Figure 4. Schematic diagram of a vapor blanket moving in vertical turbulent flow before the onset of CHF.

This rate of momentum is resisted by a lateral force,  $F_R$ , caused by the rotation of the vapor blanket due to the relative velocity between the two phases and the velocity gradient associated with the liquid boundary layer.

Just before CHF, the rate of momentum caused by evaporation into the vapor blanket is given by

$$\dot{M}_1 = \rho_G V_b^2 D_b L_m, \quad [16]$$

where  $V_b$  is the vapor velocity due to evaporation of the sublayer. The vapor velocity can be expressed as

$$V_b = \frac{q_b}{\rho_G h_{LG}}, \quad [17]$$

where  $q_b$  is the portion of the heat flux used by vaporization. For saturated flow boiling,  $q_b$  is equal to the total wall heat flux. Part of the wall flux is needed for sensible heating of the sublayer liquid in subcooled flow boiling. The heat transferred across the vapor blanket into the bulk subcooled liquid in the core is assumed to be negligible. The total heat flux,  $q$ , is equal to the subcooled heat transfer coefficient,  $h_{sc}$ , times the difference between the heated surface temperature,  $T_w$ , and the local subcooled liquid temperature,  $T_m$ , just outside the sublayer. The heat flux  $q_b$  for vaporization becomes

$$q_b = h_{sc}(T_w - T_{sat}) = q - h_{sc}(T_{sat} - T_m). \quad [18]$$

Shah (1977) presented a subcooled flow boiling heat transfer correlation for wide ranges of flow conditions and for several fluids. The subcooled heat transfer coefficient,  $h_{sc}$ , can be expressed by rearranging Shah's correlation for high boiling conditions and assuming that no heat transfer occurs between the blanket and subcooled liquid in the core region, i.e.

$$h_{sc} = \frac{230 q \text{Bo}^{0.5}}{(T_{sat} - T_m)(230 \text{Bo}^{0.5} - 1) + \frac{q}{h_L}} \quad [19]$$

where  $Bo$  is the boiling number defined as  $q/(h_{LG}G)$ , and  $h_L$  is the single-phase forced-convection heat transfer coefficient given by the well-known Dittus-Boelter equation for turbulent flow:

$$\frac{h_L D}{k_L} = 0.023 \text{Re}^{0.8} \text{Pr}_L^{0.4}, \quad [20]$$

where  $K_L$  and  $\text{Pr}_L$  are the thermal conductivity and Prandtl number of the liquid, respectively.

Where [2] and [16]–[18] are combined, the rate of momentum due to sublayer evaporation reduces to

$$\dot{M}_1 = \frac{[q - a_1 h_{sc}(T_{\text{sat}} - T_L)]^2 D_b L_m}{\rho_G h_{LG}^2}. \quad [21]$$

Beyerlein *et al.* (1985) derived an expression for the lateral force on a bubble in turbulent two-phase flow through a vertical tube. The lateral force on the vapor blanket was determined by the relative velocity of the blanket and the gradient of the liquid velocity profile (see figure 3), i.e.

$$F_R = -C \rho_L (U_b - U_{bL}) \left( \frac{\partial U_L}{\partial y} \right) \frac{\pi}{4} D_b^2 L_m, \quad [22]$$

where  $U_L$  is the local liquid velocity,  $U_{bL}$  is the mean liquid velocity at the radial position of the vapor blanket and  $C$  is a parameter which accounts for the effects of turbulent fluctuations and local bubble concentration on the rotation of the vapor blanket. Beyerlein *et al.* noted that the parameter  $C$  is a function of the average void fraction and the liquid Reynolds number, but they did not correlate or model these effects. Thus, for subcooled flow boiling with a small average void fraction, the parameter  $C$  is assumed to depend on the liquid Reynolds number, i.e.

$$C = a_2 \text{Re}^{a_3}, \quad [23]$$

where  $a_2$  and  $a_3$  are empirical constants. the local velocity gradient causing vapor blanket circulation can be approximated as the average of velocity gradients at the radial positions of  $y = \delta_m$  and  $y = \delta_m + D_b$ , i.e.

$$\frac{\partial U_L}{\partial y} = 0.379 \text{Re}^{-0.1} \frac{G}{\rho_L \delta_m} \left( 1 + \frac{\delta_m}{\delta_m + D_b} \right). \quad [24]$$

Substituting [9], [23] and [24] into [22], the lateral force can be expressed as

$$F_R = \frac{0.421 a_2 \text{Re}^{(a_3 - 0.1)} G D_b^2 L_m}{\delta_m} \left( 1 + \frac{\delta_m}{\delta_m + D_b} \right) \left( \frac{L_m \Delta \rho g}{\rho_L C_D} \right)^{0.5}. \quad [25]$$

Based on the balance between the rate of momentum of [21] and the lateral force of [25], the sublayer thickness is given by

$$\delta_m = \frac{0.421 a_2 \text{Re}^{(a_3 - 0.1)} G \rho_G h_{LG}^2 D_b}{[q_{\text{CHF}} - a_1 h_{sc}(T_{\text{sat}} - T_L)]^2} \left( 1 + \frac{\delta_m}{\delta_m + D_b} \right) \left( \frac{L_m g \Delta \rho}{\rho_L C_D} \right)^{0.5}. \quad [26]$$

CHF can then be predicted by substituting [14], [15] and [26] into [3]. A summary of the equations recommended in the numerical iteration for CHF is given in table 1.

#### 4. VERIFICATION OF THE CHF MODEL

The experimental CHF data base of the U.S.S.R. Academy of Sciences (1977) was used to evaluate the three empirical constants  $a_1$ ,  $a_2$  and  $a_3$  based on 560 data points, and to verify the accuracy of the present model for simulated PWR operating conditions. The accuracy of the model was also tested against 89 experimental CHF data points obtained from six different sources: De Bortoli (1958), Weatherhead (1963), Lee & Obertelli (1963), Matzner (1963), Thompson & Macbeth (1964) and Williams & Beus (1980).

Table 2 shows results of a sensitivity analysis of the proposed model based on various correlations for the subcooled heat transfer coefficient (Moles & Shaw 1972; Shah 1977; Gungor & Winterton 1986), the bubble drag coefficient (Harmathy 1960; Chan & Prince 1965) and the bubble departure diameter (Levy 1967; Cole & Rohsenow 1968; Smogalev 1981).

Table 1. Recommended equations for the numerical iteration of  $q_{CHF}$ 

Local conditions of $P_{sat}$ , $G$ , $(T_{sat} - T_L)$ , $D$	
INPUT PARAMETERS	<ul style="list-style-type: none"> <li>• <b>Subcooled flow boiling heat transfer coefficient</b></li> </ul> $h_{sc} = \frac{230 q_{CHF} \left( \frac{q_{CHF}}{G h_{LG}} \right)^{0.5}}{a_1 (T_{sat} - T_L) \left[ 230 \left( \frac{q_{CHF}}{G h_{LG}} \right)^{0.5} - 1 \right] + \frac{q_{CHF}}{0.023 \frac{k_L}{D} Re^{0.8} Pr_L^{0.4}}}$
	<ul style="list-style-type: none"> <li>• <b>Vapor blanket diameter</b></li> </ul> <p>Cole &amp; Rohsenow (1968): <math display="block">D_b = 1.5 \times 10^{-4} \left( \frac{\sigma}{g \Delta \rho} \right)^{0.5} \left( \frac{\rho_L c_{PL} T_{sat}}{\rho_G h_{LG}} \right)^{1.25}</math></p> <p>Smogalev (1981): <math display="block">D_b = 0.0208 \left( \frac{\sigma}{g \Delta \rho} \right)^{0.5} \left( 1 - 0.65(P_{cr} - P) \frac{\rho_G v_L G}{\rho_L \sigma g} \right)^2</math>  <math>P, P_{cr}</math> in MPa</p>
	<ul style="list-style-type: none"> <li>• <b>Bubble drag coefficient</b></li> </ul> <p>Harmathy (1960): <math display="block">C_D = \frac{2}{3} \frac{D_b}{\left( \frac{\sigma}{g \Delta \rho} \right)^{0.5}}</math></p> <p>Chan &amp; Prince (1965): <math display="block">C_D = \frac{48 \mu_L}{\rho_L D_b (U_b - U_{bl})}</math></p>
	<ul style="list-style-type: none"> <li>• <b>Vapor blanket velocity</b></li> </ul> $U_b = \left( \frac{2 L_m g \Delta \rho}{\rho_L C_D} \right)^{0.5} + 0.758 Re^{-0.1} \frac{G}{\rho_L} \left\{ \ln \left[ \frac{0.15 Re^{0.1} G \left( \delta_m + \frac{D_b}{2} \right)}{\mu_L} \right] - 0.61 \right\}$
SUBLAYER PARAMETERS	<ul style="list-style-type: none"> <li>• <b>Relative sublayer mass velocity</b></li> </ul> $G_m = \rho_L U_b$
	<ul style="list-style-type: none"> <li>• <b>Sublayer length</b></li> </ul> $L_m = \frac{2\pi\sigma(\rho_L + \rho_G)}{\rho_L \rho_G U_b^2}$
CHF	<ul style="list-style-type: none"> <li>• <b>Sublayer thickness</b></li> </ul> $\delta_m = \frac{0.421 a_2 Re^{(a_1 - 0.1)} G \rho_G h_{LG} D_b}{[q_{CHF} - a_1 h_{sc} (T_{sat} - T_L)]^2} \left( 1 + \frac{\delta_m}{\delta_m + D_b} \right) \left( \frac{\Delta \rho g L_m}{\rho_L C_D} \right)^{0.5}$
	$q_{CHF} = \frac{G_m \delta_m [h_{LG} + a_1 c_{PL} (T_{sat} - T_L)]}{L_m}$

Due to the large matrix of possible combinations of empirical models, only those combinations which gave the most accurate results are presented in table 2. The recommended correlations and corresponding values of  $a_1$ ,  $a_2$  and  $a_3$  were based on least mean deviation between predicted values and the experimental CHF data of the U.S.S.R. Academy of Sciences. Different correlations were then used for each parameter to assess the feasibility of the individual correlations.

Table 2 shows a least mean deviation of about 11.94% for the 560 data points, corresponding to subcooling from 0 to 50 K. The value of 0.35 of the empirical constant  $a_1$  indicates that the subcooling of the liquid, as it enters the sublayer, is 35% of bulk liquid subcooling. Table 2 also shows that the least mean deviations of the present model and the W-3 correlation (Tong 1972) for 89 water data points obtained from six sources are 13.37 and 13.4%, respectively. The W-3 correlation, which includes 17 empirical constants is popular in predicting the subcooled flow boiling CHF for PWR thermal-hydraulic design.

Table 2 shows that the bubble departure diameter correlations of Cole & Rohsenow (1968) and Smogalev (1981) offer good accuracies in predicting the CHF data, while Levy's (1967) model is unsuccessful in correlating the constants of the model.

Figures 5(a, b) show comparisons of the predicted CHF based on the values of  $a_1$ ,  $a_2$  and  $a_3$  given in table 2 to 140 data points (U.S.S.R. Academy of Sciences 1977) corresponding to a tube diameter

Table 2. Comparison of predictions of the present model and the W-3 correlation (Tong 1968)

Parameter	Reference	a <sub>1</sub>	a <sub>2</sub>	a <sub>3</sub>	Water <sup>a</sup>		Water <sup>b</sup>		
					MD (%)	AD (%)	MD (%)	AD (%)	
PRESENT MODEL	Subcooled heat transfer coefficient	Moles & Shaw (1972)	0.60	240	-0.8	12.24	1.74	13.55	0.94
		Shah (1977) <sup>c</sup>	0.35	240	-0.8	11.94	1.63	13.37	-1.34
		Gungor & Winterton (1986)	0.50	240	-0.8	13.12	0.17	12.83	-1.50
	Bubble drag coefficient	Harmathy (1960)	0.35	8	-0.8	16.88	-1.90	7.63	-0.51
		Chan & Prince (1965) <sup>c</sup>	0.35	240	-0.8	11.94	1.63	13.37	-1.34
	Bubble departure diameter	Levy (1967)	0.35	10	-0.8	33.93	1.14	18.24	1.02
Cole & Rohsenow (1968) <sup>c</sup>		0.35	240	-0.8	11.94	1.63	13.37	-1.34	
Smogalev (1981)		0.35	56	-0.8	17.45	-5.33	12.38	-1.58	
W-3	Tong (1968)	—	—	—	—	—	13.40	7.18	

<sup>a</sup>U.S.S.R. Academy of Sciences (1977);  $\rho_G/\rho_L = 0.031-0.218$ ; 560 data points.  $P = 4.9-17.6$  MPa,  $G = 1000-5000$  kg/m<sup>2</sup>s,  $D = 4-16$  mm,  $\Delta T_{sub} = 0-50$  K for tube diameters other than 8 mm,  $q_{CHF} = q_{CHF, 8mm}(8/D)^{0.5}$ .

<sup>b</sup>References for experimental data: De Bortoli (1958), Weatherhead (1963), Lee & Obertelli (1963), Matzner (1963), Thompson & Macbeth (1964), Williams & Beus (1980); 89 data points.  $P = 6.89-15.76$  MPa,  $G = 1350-5200$  kg/m<sup>2</sup>s,  $D = 5.7-12.8$  mm,  $\Delta T_{sub} = 2-59$  K.

<sup>c</sup>Recommended correlation used in figures 5(b), 6(b) and 7-12.

of 8 mm. It is evident that the Chan & Prince (1965) model for the bubble drag coefficient gives better results than that of Harmathy (1960). This is, perhaps, due to the strong influence of viscous forces on bubble motion at high pressures.

Figures 6(a, b) show comparisons of the predicted CHF to 89 data points obtained from the six data sources listed in table 2. The Chan & Prince model shows some departure from low-pressure data points where viscous forces are less significant than buoyancy forces. This indicates that the Harmathy model may be more appropriate for lower pressures than the Chan & Prince model.

5. PARAMETRIC TRENDS

The parametric trends of the subcooled CHF vary according to the thermal-hydraulic conditions determined by the combination of the various ranges of pressure, mass velocity, subcooling and

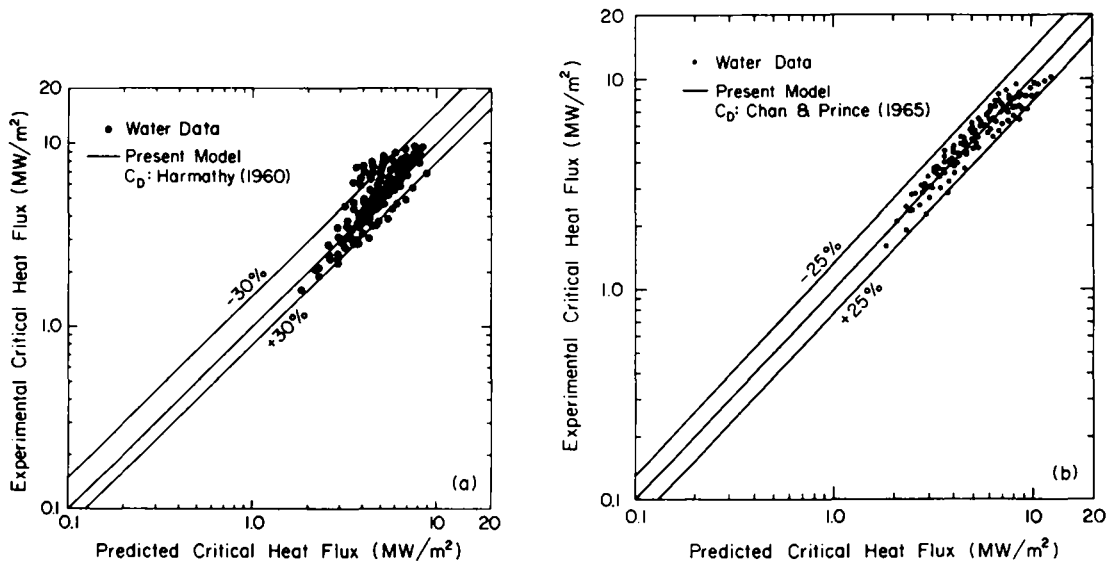


Figure 5. Comparison of experimental CHF data for water (U.S.S.R. Academy of Sciences 1977) with present model predictions based on the bubble drag coefficient relations of (a) Harmathy (1960) and (b) Chan & Prince (1965).

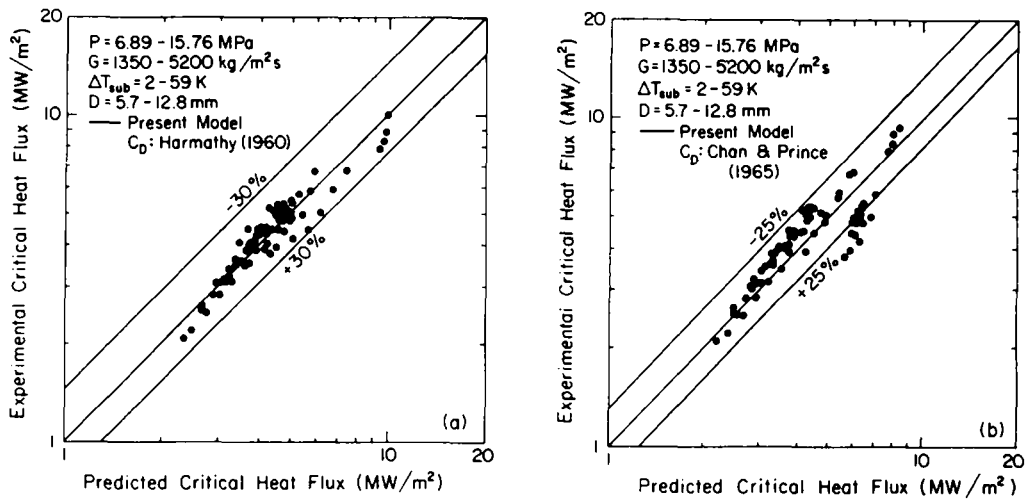


Figure 6. Comparison of experimental CHF data for water obtained from six sources (see table 2) with model predictions based on the bubble drag coefficient relations of (a) Harmathy (1960) and (b) Chan & Prince (1965).

tube diameter. The parametric trends of high pressure, high mass velocity, medium subcooling and small tube diameter, typical of PWR operating conditions (Bergles 1963, 1977, 1979; Tong 1965, 1972; Gambill 1968; Ornatskiy 1969; Tolubinskiy *et al.* 1970; Tolubinskiy & Motorin 1973; Doroshchuk *et al.* 1975; Collier 1980), can be briefly summarized as follows:

- CHF increases with increasing mass velocity.
- CHF decreases with increasing pressure.
- CHF increases with increasing degree of subcooling.
- CHF increases with smaller tube diameters.

Equation [3] shows that CHF is proportional to the sublayer thickness  $\delta_m$ , the relative sublayer mass velocity  $G_m$  and the sum of sensible and latent heat  $\Delta H$ ; and is inversely proportional to the length of the vapor blanket  $L_m$ .

Figure 7 shows the normalized data of the length of the sublayer, the sublayer thickness, the relative sublayer mass velocity, the sensible plus latent heat, the predicted CHF and the

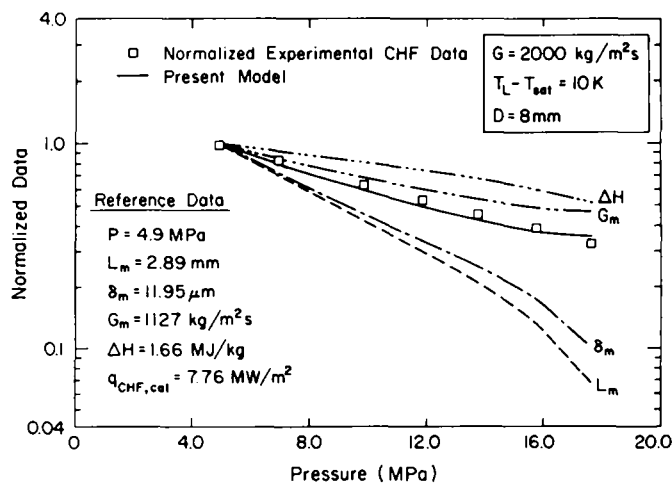


Figure 7. Pressure effect on CHF at 2000 kg/m<sup>2</sup>s mass velocity and 10 K subcooling for an 8 mm dia tube.

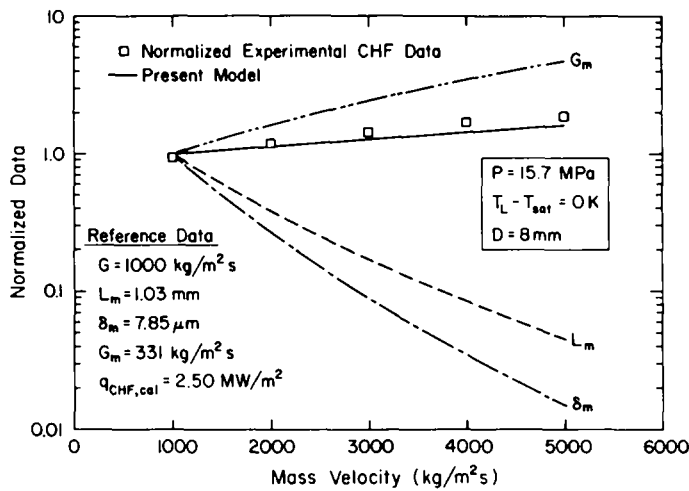


Figure 8. Mass velocity effect on CHF at 15.7 MPa pressure and 0 K subcooling for an 8 mm dia tube.

experimental CHF (U.S.S.R. data for an 8 mm tube) as the pressure is increased from 4.9 to 17.6 MPa at 2000 kg/m<sup>2</sup>s mass velocity and 10 K subcooling, inside an 8 mm dia tube based on reference data at a pressure of 4.9 MPa. The sublayer thickness, the relative sublayer mass velocity, the length of the vapor blanket and the subcooling latent heat decrease with increasing pressure. The normalized ratios of the sublayer thickness and the length of the vapor blanket vary from 1.0 to 0.067 and 1.0 to 0.099, respectively, as pressure increases from 4.9 to 17.6 MPa. Yet, the net influence of the ratio  $\delta_m/L_m$  in [3] on CHF is not a very strong function of pressure. Thus, the decrease of the relative sublayer mass velocity, the enthalpy and the ratio of sublayer thickness to blanket length with increasing pressure determines the pressure trend of CHF.

Figure 8 shows predicted and experimental CHF values at 15.7 MPa pressure and 0 K subcooling for an 8 mm dia tube based on reference data at 1000 kg/m<sup>2</sup>s mass velocity. The normalized ratio of the sublayer thickness to the length of the vapor blanket decreases to 0.33, and the normalized relative sublayer mass velocity increases to 4.72 when mass velocity is increased from 1000 to 5000 kg/m<sup>2</sup>s. The dominating influence of relative sublayer mass velocity results in an increase in CHF with increasing mass velocity.

Figure 9 shows that with an increase in subcooling from 0 to 50 K, the normalized ratios of the sublayer thickness, the relative sublayer mass velocity and enthalpy increase to 1.296, 1.091 and

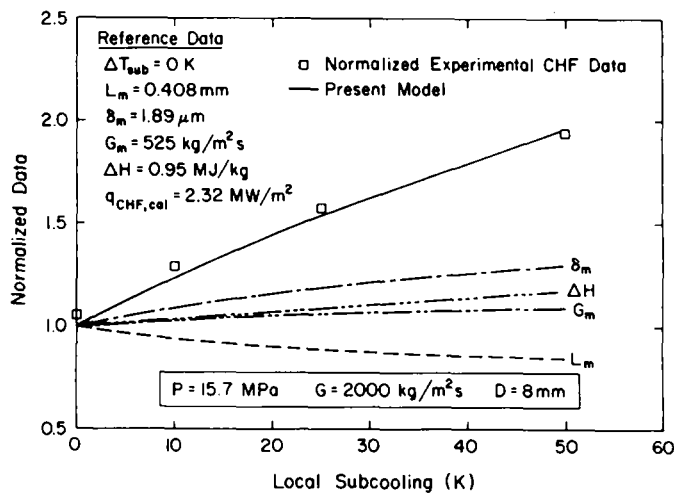


Figure 9. Subcooling effect on CHF at 15.7 MPa pressure and 2000 kg/m<sup>2</sup>s mass velocity for an 8 mm dia tube.

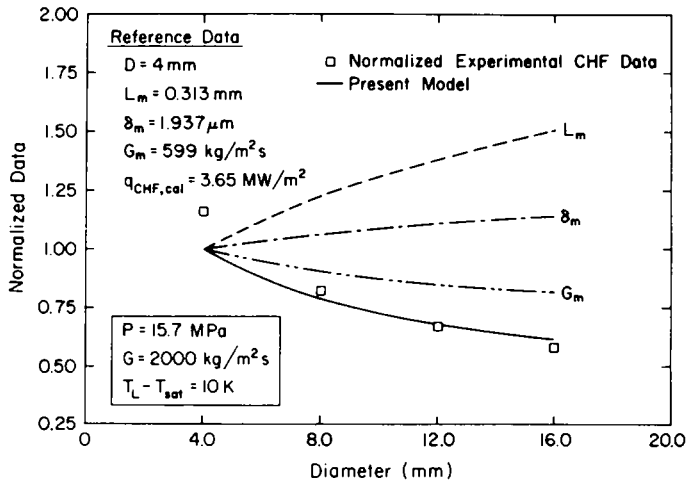


Figure 10. Diameter effect on CHF at 15.7 MPa pressure, 2000 kg/m<sup>2</sup>s mass velocity and 10 K subcooling.

1.171, respectively, while the normalized ratio of the vapor blanket length decreases to 0.843. Thus, the net effect is an increase of CHF with increased subcooling.

Figure 10 shows that the decrease of CHF with increasing tube diameter is caused by the dominant decrease of the term  $G_m L_m$  in [3].

Figure 11 shows a comparison of predicted CHF based on the present model and the W-3 correlation with experimental data obtained at the U.S.S.R. Academy of Sciences and recent data obtained by the authors at the Institute of Nuclear Energy Research, Taiwan, R.O.C. The model displays accuracy far superior to the W-3 correlation in predicting both the CHF values and the trend of CHF with pressure.

The parametric trends shown in figures 7–11 are evidence that the proposed model is very accurate in predicting independent CHF variations with respect to pressure, mass velocity, local subcooling and tube diameter. The figures also indicate that the variation of CHF resulting from changes in any of these parameters can be explored by studying the net influence of the parameter on the sublayer thickness, the blanket length, the relative mass velocity and the subcooling of the sublayer liquid.

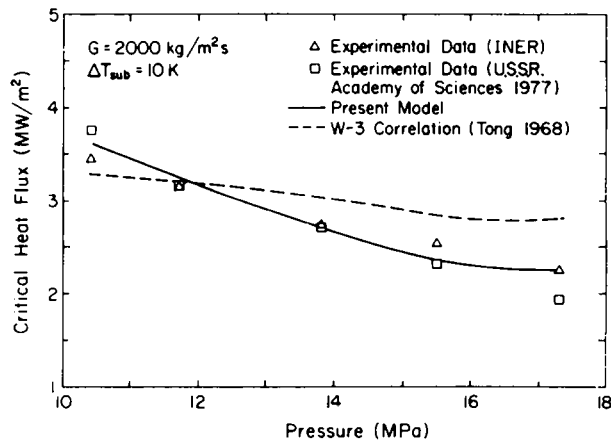


Figure 11. Comparison of predicted CHF with experimental data for water obtained by the authors at the Institute of Nuclear Energy Research (INER), Taiwan, R.O.C.

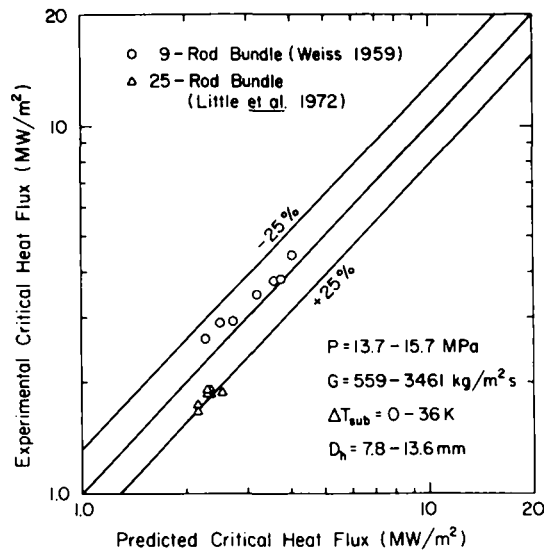


Figure 12. Comparison of predicted CHF to experimental data for water in 9-rod (Weiss 1959) and 25-rod bundles (Little *et al.* 1972).

## 6. APPLICATION OF THE CHF MODEL TO PWR CORE THERMAL DESIGN

Typically, the subcooled core flow in the PWR vessel is upward from the lower plenum, through the fuel bundles associated with a non-uniform axial heat flux distribution, to the upper plenum. The inputs of the present model are local bulk conditions of pressure, mass velocity, subcooling and diameter. Therefore, the accuracy of the model is independent of the axial heat flux distribution along the flow channel.

Figure 12 shows a comparison of the predicted and experimental CHF for a 9-rod bundle (Weiss 1959) and a 25-rod bundle (Little *et al.* 1972) using an equivalent hydraulic diameter of the bundles. The good agreement between the model predictions and experimental data indicates that the present model is particularly useful in thermal-hydraulic computer programs, such as COBRA IV-I (Wheeler 1976) and THINC IV (Chu *et al.* 1973), which provide instantaneous *local* conditions for design and safety analyses of PWRs.

## 7. CONCLUSIONS

A new mechanistic CHF model has been developed for vertical subcooled flow at high pressure and high mass velocity. This model is based on the observation that, during fully developed boiling, a vapor blanket forms in the vicinity of the heated wall by the coalescence of small bubbles, leaving a thin liquid sublayer in contact with the heated wall beneath the blanket. The onset of sublayer dryout was assumed to be triggered by a Helmholtz instability at the sublayer-vapor blanket interface, and CHF was postulated to occur when the rate of heat supplied at the wall exceeded the enthalpy of fresh liquid entering the sublayer from the bubbly layer and core regions.

The proposed model supports the hypothesis that the parametric trends of CHF with varying ranges of pressure, mass velocity, subcooling and tube diameter can be explored by analyzing the net effect of each of these parameters on the sublayer thickness, the sublayer length, the sublayer relative mass velocity and the enthalpy of liquid entering the sublayer.

The validity of the CHF model was demonstrated by the close agreement between model predictions and experimental data for water at simulated PWR conditions. The accuracy of the model is independent of the axial heat flux distribution association with PWR rod bundles since the inputs of the model are local bulk flow conditions of pressure, mass velocity, subcooling and tube diameter. Thus, the proposed model is particularly useful in thermal-hydraulic computer programs which provide instantaneous local conditions for the design and safety analyses of PWRs.

## REFERENCES

- ARPACI, V. S. & LARSEN, P. S. 1984 *Convection Heat Transfer*. Prentice-Hall, Edgewood Cliffs, N.J.
- BERGLES, A. E. 1963 Subcooled burnout in tube of small diameter. ASME Paper 63-WA-182.
- BERGLES, A. E. 1977 Burnout in boiling heat transfer, part II: subcooled and low quality forced convection systems. *Nucl. Saf.* **18**, 154–167.
- BERGLES, A. E. 1979 Burnout in boiling heat transfer, part III: high quality forced convection systems. *Nucl. Saf.* **20**, 671–689.
- BEYERLEI, S. W., COSSMANN, R. K. & RICHTER, H. J. 1985 Prediction of bubble concentration profiles in vertical turbulent two-phase flow. *Int. J. Multiphase Flow* **11**, 629–641.
- BHAT, A. M. PRAKASH, R. & SAINI, J. S. 1983 Heat transfer in nucleate pool boiling at high heat flux. *Int. J. Heat Mass Transfer* **26**, 833–840.
- CHAN, B. K. C. & PRINCE, R. G. H. 1965 Viscous drag on a gas bubble rise in a liquid. *AIChE JI* **11**, 188–192.
- CHU, P. T., CHELEMER, H., HOCHREITER, L. E. & TONG, L. S. 1973 THINC-IV, An improved program for thermal-hydraulic analysis of rod bundle cores. Westinghouse Electric Co. Report WCAP-7956, Pittsburgh, Pa.
- COLE, R. & ROHSENOW, W. R. 1968 Correlation of bubble departure diameters for boiling of saturated liquids. *Chem. Engng Prog. Symp.* **92**, 211–213.
- COLLIER, J. G. 1980 *Convective Boiling and Condensation*, 2nd edn. McGraw-Hill, London.
- DE BORTOLI, R. A. 1958 Forced convection heat transfer burnout studies for water in rectangular channels and round tubes at pressures above 500 psia. Westinghouse Electric Co. Report WAPD-188, Pittsburgh, Pa.
- DOROSHCHUK, V. E., LEVITAN, L. L. & LANTZMAN, F. P. 1975 Investigation into burnout in uniformly heated tubes. ASME Paper 75-WA/HT-22.
- FIORI, M. P. & BERGLES, A. E. 1970 Model of critical heat flux in subcooled flow boiling. *Proc. 4th Heat Transfer Conf., Versailles* **9**, 354–355.
- GAMBILL, W. R. 1968 Burnout in boiling heat transfer- Part II. *Nucl. Saf.* **9**, 467–480.
- GROENEVELD, D. C. & SNOEK, C. W. 1984 A comprehensive examination of heat transfer correlation suitable for reactor safety analysis. *Multiphase Sci. Technol.* **2**, 1–107.
- GUNGOR, K. E. & WINTERTON, R. H. S. 1986 A general correlation for flow boiling in tubes and annuli. *Int. J. Heat Mass Transfer* **29**, 351–358.
- HARAMURA, Y. & KATTO, Y. 1983 A new hydrodynamic model of critical heat flux, applicable widely to both pool and forced convection boiling submerged bodies in saturated liquids. *Int. J. Heat Mass Transfer* **26**, 389–399.
- HARMATHY, T. Z. 1960 Velocity of large drops and bubbles in media of infinite and restricted extent. *AIChE JI* **6**, 281–288.
- HEWITT G. F. 1978 Critical heat flux in flow boiling. *Proc. 6th Int. Heat Transfer Conf., Toronto, Ont.* **6**, 143–172.
- HINO, R. & UEDA, T. 1985 Studies on heat transfer and flow characteristics in subcooled flow boiling—Part 2, flow characteristics. *Int. J. Multiphase Flow* **11**, 283–297.
- ISHII, M. & ZUBER, N. 1979 Drag coefficient and relative velocity in bubbly, droplet or particulate flows. *AIChE JI* **25**, 843–854.
- KITTO, J. B. JR 1980 Critical heat flux and limiting quality phenomenon. *AIChE Symp. Ser.* **76**, 57–78.
- KOUMOUTSOS, N., MOISSIS, R. & SPYRIDONOS, A. 1968 A study of bubble departure in forced-convection boiling. *J. Heat Transfer* **90**, 223–230.
- KUTATELADZE, S. S. 1966 The concept of a fluid with disappearing viscosity and some problems of phenomenological theory of turbulence near the wall. *Proc. 3rd Int. Heat Transfer Conf., Chicago, Ill.* **3**, 1–6.
- LAHEY, R. T. JR & MOODY, F. J. 1977 *The Thermal Hydraulics of a Boiling Water Nuclear Reactor*. ANS Publications, La Grange Park, Ill.
- LEE, D. H. & OBERTELLI, J. D. 1963 An experimental investigation of forced convection burnout in high pressure water, Part I. U.K. Atomic Energy Authority Report AEEW-R-356, Winfrith, Dorset.

- LEVY S. 1966 Forced-convection subcooled boiling prediction of vapor volumetric fraction. General Electric Co. Report GEAP-5157, San Jose, Calif.
- LEVY, S. 1967 Forced-convection subcooled boiling prediction of vapor volumetric fraction. *Int. J. Heat Mass Transfer* **10**, 951-965.
- LITTLE, R. B., OBERTELLI, J. D. & ROBINSON, G. H. 1972 Dryout experiments in a 25-rod 12 feet long bundle under PWR and other conditions. U.K. Atomic Energy Authority Report AEEW-R779, Winfrith, Dorset.
- MATTSON, R. J., HAMMITT, F. G. & TONG, L. S. 1973 A photographic study of the subcooled flow boiling crisis in Freon-113. ASME Paper 73-HT-39.
- MATZNER, B. 1963 Basic experimental studies of boiling fluid flow and heat transfer at elevated pressures. U.S. Atomic Energy Commission Report TID 18978, Washington, D.C.
- MESLER, R. 1976. A mechanism supported by extensive experimental evidence to explain high heat fluxes observed during nucleate boiling. *AIChE JI* **22**, 246-252.
- MOLEN, S. B. V. & GALJEE, F. W. B. M. 1978 The boiling mechanism during burnout phenomena in subcooled two phase water flow. *Proc. 6th Int. Heat Transfer Conf, Toronto, Ont.* **1**, 381-385.
- MOLES, F. D. & SHAW, J. F. G. 1972 Boiling heat transfer to subcooled liquids under conditions of forced convection. *Trans. Instn chem. Engrs* **50**, 76-83.
- MUDAWWAR, I. A., INCROPERA, T. A. & INCROPERA, F. P. 1987 Boiling heat transfer and critical heat flux in liquid films falling on vertically-mounted heat sources. *Int. J. Heat Mass Transfer* **30**, 2083-2095.
- ORNATSKIY, A. P. 1969 The effect of basic regime parameters and channel geometry on critical heat fluxes in forced convection of subcooled water. *Heat Transfer -Soviet Res.* **1**, 17-22.
- PURCUPILE, J. C. & GOUSE, S. W. JR 1972 Reynolds flux model of critical heat flux in subcooled forced convection boiling. ASME Paper 72-HT-4.
- SERIZAWA, A. 1983 Theoretical prediction of maximum heat flux in power transients. *Int. J. Heat Mass Transfer* **26**, 921-932.
- SHAH, M. M. 1977 A general correlation for heat transfer during subcooled boiling in pipes and annuli. *ASHRAE Trans.* **83**, 202-217.
- SMOGALEV, I. P. 1981 Calculation of critical heat fluxes with flow of subcooled water at low velocity. *Therm. Engng* **28**, 208-211.
- STYRIKOVICH, M. A., NEVSTRUEVA, E. I. & DVORINA, G. M. 1970 The effect of two phase flow pattern on the nature of heat transfer crisis in boiling. *Proc. 4th Int. Heat Transfer Conf., Versailles* **9**, 360-362.
- THOMPSON, B. & MACBETH, R. V. 1964 Boiling water heat transfer—burnout in uniformly heat round tubes: a compilation of world data with accurate correlations. U.K. Atomic Energy Authority Report AEEW-R-356, Winfrith, Dorset.
- THEOFANOUS, T. G. 1980 The boiling crisis in nuclear reactor safety and performance. *Int. J. Multiphase Flow* **6**, 69-95.
- TOLUBINSKIY, V. I. & MATORIN, A. S. 1973 Forced convection boiling heat transfer crisis with binary mixture. *Heat Transfer—Soviet Res.* **5**, 98-101.
- TOLUBINSKIY, V. I., LITOSHENKO, A. K. & SHEVTSOV, V. L. 1970 Effect of pressure on the magnitude of the critical heat flux density. *Heat Transfer—Soviet Res.* **2**, 191-194.
- TONG, L. S. 1965 *Boiling Heat Transfer and Two Phase Flow*. Wiley, New York.
- TONG, L. S. 1968 An evaluation of departure from nucleate boiling in bundles of reactor fuel rods. *Nucl. Sci. Engng* **33**, 7-15.
- TONG, L. S. 1972 Boiling crisis and critical heat flux. U.S. Atomic Energy Commission Report TID-25887, Washington, D.C.
- TONG, L. S. 1975 A phenomenological study of critical heat flux. ASME Paper 75-HT-68.
- TONG, L. S. & HEWITT, G. F. 1972 Overall viewpoint of flow boiling CHF mechanisms. ASME Paper 52-HT-54.
- U.S.S.R. Academy of Sciences 1977 Tabular data for calculating burnout when boiling water in uniformly heat round tubes. *Therm. Engng* **23**, 77-79.
- WEATHERHEAD, R. J. 1963 Nucleate boiling characteristics and the critical heat flux occurrence in subcooled axial flow water system. Argonne National Lab. Report ANL-6675, Argonne, Ill.

- WEISMAN, J. & PEI, B. S. 1983 Prediction of critical heat flux in flow boiling at low qualities. *Int. J. Heat Mass Transfer* **26**, 1463–1477.
- WEISMAN, J. & YING, S. H. 1983 Theoretically based CHF prediction at low qualities and intermediate flows. In *Proc. 1st Nuclear Thermohydraulics Winter Mtg, San Francisco, Calif.* **1**, 65–72.
- WEISMAN, J. & YING, S. H. 1985 A theoretically based critical heat flux prediction for rod bundles at PWR conditions. *Nucl. Engng Des.* **85**, 239–250.
- WEISS, A. 1959 Results of final heat flux tests at 2000 psia on parallel rods. Westinghouse Electric Co. Report WAPD-TH478, Pittsburgh, Pa.
- WHEELER, C. L. 1976 COBRA-IV-I; an interim version of COBRA for thermal hydraulic analysis of rod bundle nuclear fuel elements and cores. Battelle Northwest Pacific Lab. Report BNWL-1962, Richland, Wash.
- WILLIAMS, C. L. & BEUS, S. G. 1980 Critical heat flux experiments in a circular tube with heavy water and light water. Westinghouse Electric Co. Report WAPD-TM-1462, Pittsburgh, Pa.